Received: 10 April 2018 | Revised: 7 September 2018 | Accepted: 13 September 2018

DOI: 10.1111/fog.12415

ORIGINAL ARTICLE

WILEY FISHERIES OCEANOGRAPHY

Spatial variability in ocean-mediated growth potential is linked to Chinook salmon survival

Mark Henderson[1] | Jerome Fiechter[2] | David D. Huff[3] | Brian K. Wells[4]

[1]U.S. Geological Survey, California Cooperative Fish and Wildlife Research Unit, Department of Fisheries Biology, Humboldt State University, Arcata, California

[2]Department of Ocean Sciences, University of California at Santa Cruz, Santa Cruz, California

[3]Estuary and Ocean Ecology Program, Fish Ecology Division, Northwest Fisheries Science Center, National Oceanic and Atmospheric Administration, Hammond, Oregon

[4]Fisheries Ecology Division, Southwest Fisheries Science Center, National Marine Fisheries Service, National Oceanic and Atmospheric Administration, Santa Cruz, California

Correspondence
Mark Henderson, U.S. Geological Survey, California Cooperative Fish and Wildlife Research Unit, Department of Fisheries Biology, Humboldt State University, Arcata, CA.
Email: mark.henderson@humboldt.edu

Funding information
National Aeronautics and Space Administration, Grant/Award Number: 80NSSC17K0574; California Current Integrated Ecosystem Assessment; National Science Foundation, Grant/Award Number: OCE-1566623

Abstract

Early ocean survival of Chinook salmon, *Oncorhynchus tshawytscha*, varies greatly inter-annually and may be the period during which later spawning abundance and fishery recruitment are set. Therefore, identifying environmental drivers related to early survival may inform better models for management and sustainability of salmon in a variable environment. With this in mind, our main objectives were to (a) identify regions of high temporal variability in growth potential over a 23-year time series, (b) determine whether the spatial distribution of growth potential was correlated with observed oceanographic conditions, and (c) determine whether these spatial patterns in growth potential could be used to estimate juvenile salmon survival. We applied this method to the fall run of the Central Valley Chinook salmon population, focusing on the spring and summer period after emigration into central California coastal waters. For the period from 1988 to 2010, juvenile salmon growth potential on the central California continental shelf was described by three spatial patterns. These three patterns were most correlated with upwelling, detrended sea level anomalies, and the strength of onshore/offshore currents, respectively. Using the annual strength of these three patterns, as well as the overall growth potential throughout central California coastal waters, in a generalized linear model we explained 82% of the variation in juvenile salmon survival estimates. We attributed the relationship between growth potential and survival to variability in environmental conditions experienced by juvenile salmon during their first year at sea, as well as potential shifts in predation pressure following out-migration into coastal waters.

1 | INTRODUCTION

Survival of juvenile Chinook salmon, *Oncorhynchus tshawytscha*, from California's Central Valley varies by at least 20-fold, and it is believed that cohort strength is likely set shortly after emigration to the coastal ocean (Beamish and Mahnken, 2001, Kilduff, Botsford, & Teo, 2014; Wells et al., 2017). A portion of the variability in first-year survival can be attributed to freshwater conditions (Michel et al., 2015), but ocean conditions that affect salmon prey availability have also been implicated in recruitment dynamics (Lindley et al., 2009; Wells et al., 2016). The initial period at sea is associated with peak rates of energy accumulation and growth for juvenile Chinook salmon (MacFarlane, 2010), and availability of krill is associated with increased survival of the out-migrating juveniles (Wells et al., 2012, 2016). In years with reduced ocean productivity, salmon experience higher size-selective mortality (Woodson et al., 2013) as well as increased predation pressure from predators with insufficient alternative prey resources (Wells et al., 2017).

To examine the effects of oceanographic conditions on salmon growth, previous studies have used a combination of lower trophic level ecosystem models and bioenergetics models (Fiechter et al.,

2015; Kishi, Kaeriyama, Ueno, & Kamezawa, 2010; Yoon, Watanabe, Ueno, & Kishi, 2015). These lower trophic level ecosystem models estimate prey availability as a function of oceanic currents, water temperatures, and primary productivity. Simulated prey availability and water temperature is then used to estimate salmon growth using the bioenergetics model. For example, Fiechter et al. (2015) used such an approach to demonstrate that salmon growth was improved during out-migration years when early season upwelling was intensified and led to more persistent primary and secondary production throughout the upwelling season. These previous studies provide valuable information on how prey availability influences salmon growth and distribution, but they do not readily provide a means to estimate juvenile salmon survival as a function of oceanographic conditions.

Gaining a better understanding of how oceanic processes influence juvenile salmon survival will provide a means to more accurately predict adult returns and assist the development of more robust management policies. With this in mind, the main objectives of our analysis were to (a) identify regions of high temporal variability in growth potential over a 23-year time series, (b) correlate these spatial growth potential patterns with observed oceanographic conditions, and (c) determine whether these spatial patterns in growth potential could be used to estimate juvenile salmon survival. Our analysis combined multiple physical, biological, and statistical modeling methods to identify primary drivers of juvenile salmon survival. We applied this approach to the fall run of the Central Valley Chinook salmon population (Lindley et al., 2009), focusing on the spring and summer months after emigration into central California coastal waters (Figure 1).

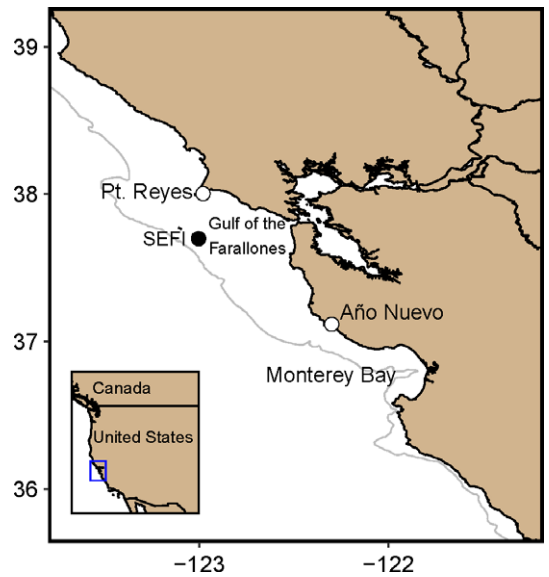

FIGURE 1 Coastal central California with Pt Reyes and Año Nuevo (white circles), Southeast Farallon Islands (SEFI; black circle), Gulf of the Farallones, and Monterey Bay shown. Gray contour is the 200 m isobaths

2 | METHODS

2.1 | Overview

We combined multiple modeling and analytical methods to ascertain whether we could estimate juvenile salmon survival off the central California coast as a function of oceanographic conditions. We used a regional ocean circulation model to estimate hydrodynamic variables (e.g., currents and temperatures). Output from the physical model served as input for a biogeochemical model used to estimate primary and secondary production. Temperature estimates from the physical model and secondary production (i.e., krill) from the biogeochemical model were used in a bioenergetics model to estimate juvenile salmon growth potential over a 23-year time series in 167 spatial cells throughout the study area. We then applied a multivariate analysis to represent variability of 167 spatial cells throughout the time series into a reduced number of dimensions. Finally, the results from the multivariate analysis were used as independent variables in a generalized linear model to estimate survival as a function of the spatial variability in growth potential. Our response in the generalized linear model was survival estimated from coded-wire tag recoveries.

2.2 | Physical–biogeochemical and bioenergetics models

To determine juvenile salmon growth potential, we used an existing data assimilative implementation of the Regional Ocean Modeling System (ROMS) at 1/10° horizontal resolution (~10 km) for the broader California Current region (i.e., the 1980–2010 ocean circulation reanalysis of Neveu et al., 2016) and a modified version of the North Pacific Ecosystem Model for Understanding Regional Oceanography (NEMURO) biogeochemical model (Fiechter et al., 2015; Kishi et al., 2007). ROMS is a hydrostatic, primitive equation model that uses terrain-following coordinates in the vertical and orthogonal curvilinear coordinates in the horizontal (Shchepetkin & McWilliams, 2005). Its advanced numerical algorithms and grid structure make ROMS well suited to model coastal regions characterized by complex bathymetry and coastlines (Haidvogel et al., 2008). The NEMURO biogeochemical model, which was specifically developed to represent lower trophic level ecosystem processes in the North Pacific, includes three limiting macronutrients (nitrate, ammonium and silicic acid), two phytoplankton size-classes (nanophytoplankton and diatoms), three zooplankton size-classes (micro-, meso-, and krill), and three detritus pools (dissolved and particulate organic nitrogen and particulate silica).

Calculations within NEMURO are driven by stored daily-averaged oceanic fields and surface atmospheric fluxes output from the ROMS reanalysis (Fiechter, Edwards, & Moore, 2018). One significant advantage of using the reanalysis is it provides improved physical ocean state estimates and consistent atmospheric forcing

via state-of-the-art data assimilation techniques (Moore et al., 2011) and should allow for an improved representation of regional- and basin-scale influences (e.g., Crawford et al., 2017; Jacox, Moore, Edwards, & Fiechter, 2014) on the local-scale circulation. We focus on the period 1988–2010 for which the reanalysis was forced with the relatively high-resolution (0.25°) Cross-Calibrated Multi-Platform (CCMP) winds (Atlas et al., 2011).

Growth conditions were approximated by substituting mean sea surface temperature and krill concentrations from the physical–biogeochemical model directly into a salmon bioenergetics model previously configured for Central Valley juvenile Chinook salmon (Fiechter et al., 2015). The bioenergetics model is adapted from the dynamic energy budget (DEBkiss) model of Jager, Martin, and Zimmer (2013), where growth is given by the difference between the biomass assimilated and that expended on maintenance metabolism and swimming. Mass-specific biomass assimilation (J_A) was calculated with the following equation:

$$J_A = y_{XA} * F * j_{X_m} * e^{dT} * W^{\frac{2}{3}} \quad (1)$$

where y_{XA} is the conversion efficiency for assimilated energy (0.8 based on Jager et al., 2013), F is a Holling's type II functional response that is dependent on prey biomass density, j_{X_m} is the maximum surface area-specific feeding rate (0.229 based on MacFarlane, 2010), d is the temperate coefficient for biomass assimilation (0.068 based on Stewart and Ibarra, 1991), T is water temperature, and W is the fish body mass. The cost of maintenance metabolism and the metabolic costs of swimming (based on a movement speed of 1 body length per second) were subtracted from the assimilated biomass and multiplied by a growth conversion efficiency of 0.8 (Jager et al., 2013) to calculate somatic growth. Full equations and parameter values are provided in Fiechter et al. (2015) supplemental material. The resulting mean growth potential values for April–September (i.e., the spring and summer growth period for juvenile fall-run Chinook salmon) were calculated for each 10 × 10 km spatial cell in the ROMS domain off central California (n = 167) for 1988–2010. We then used these growth potential estimates to identify dominant modes of variability throughout the time series using non-metric multidimensional scaling (NMS).

2.3 | Observed distribution of Chinook salmon

We used empirical observations to evaluate spatial occupancy of juvenile Chinook salmon throughout our study area. Juvenile salmon were collected during the summers of 1997–2005, 2007, and 2010–2013 from 36.5°N to 39.0°N following methods in Harding, Ammann, and MacFarlane (2011) and Hassrick et al. (2016). In summary, a Nordic 264 Rope Trawl with 14 m vertical and 27 m horizontal mouth dimensions was towed at the surface for an average of 22 min at an average speed of 6.5 km/hr. The codend liner retained any fish >40 mm. We considered any Chinook salmon less than 200 mm as juveniles experiencing their first summer at sea (Woodson et al., 2013).

2.4 | Non-metric multidimensional scaling

Spatially varying growth potential relationships among years were described objectively by plotting an NMS (Kruskal, 1964; Mather, 1976) ordination based on Euclidean distances among spatial cells across the years in the data set (years in rows and spatial cells in columns). Prior to analysis, we transformed data using the Wisconsin double standardization where spatial cells were first standardized by their maxima and then years were standardized by the mean April - September growth. This analysis was implemented with the R statistical program (R Core Team 2016) using the "vegan" package (Oksanen et al., 2017). NMS is an unconstrained ordination method that maps multidimensional data (spatial cells, in this case) into a reduced dimensional space using the rank order of dissimilarity values among samples McCune, Grace, and Urban (2002). The optimum ordination configuration was determined by using multiple random starts to maximize the likelihood of finding a global minimum stress value. Stress, calculated as the difference between the reduced dimensional ordination and the original data set, was used to determine model fit. As a general rule of thumb, stress values larger than 0.2 indicate poor model fit, values less than 0.2 are reasonable but may be misleading, values less than 0.1 represent a good ordination and are unlikely to lead to false inferences, and values less than 0.05 correspond to an excellent representation with no possibility of misinterpretation (Clarke, 1993). The appropriate number of dimensions was determined by examining stress as a function of dimensionality and selecting the dimension beyond which there was no appreciable reduction in stress.

2.5 | Oceanographic indices

To explore how the observed spatial variability in growth potential related to observed oceanographic conditions, we examined relationships between NMS ordination scores and a number of oceanographic indicators using Pearson correlations and the *envfit* function in the "vegan" package. The oceanographic indicators included (a) Bakun's upwelling index, (b) the Oceanic Niño Index (ONI), (c) the Pacific Decadal Oscillation (PDO), (d) The Northern Oscillation Index (NOI), (e) The North Pacific Gyre Oscillation (NPGO), (f) the mean sea level at San Francisco, (g) ROMS estimated mean strength of the eastward (~onshore) velocity component off San Francisco, and (h) ROMS estimated mean strength of the northward (~alongshore) velocity component off San Francisco. Upwelling, which is caused by wind stress in combination with the Earth's rotation (Bakun, 1973), brings colder, nutrient-rich deep waters to the surface. The influx of these nutrient-rich waters is associated with increased biological productivity and the growth and survival of juvenile salmon (Wells et al., 2012, 2016). Bakun's upwelling index values (Bakun, 1973; Schwing, O'Farrell, Steger, & Baltz, 1996) were obtained from monthly upwelling values representing the months March–June offshore of Point Arena (39.0°N) (https://www.pfeg.noaa.gov/products/PFELData/upwell/monthly/upindex.mon). The Oceanic Niño Index (ONI) is a three-month running mean of SST anomalies averaged over the Niño

3.4 region of 5°S–5°N and 120°W–170°W, with positive values representing more El Niño-type conditions (Null, 2017). Persistent changes in the ONI index can lead to physical and trophic changes in the California Current Ecosystem (Peterson et al., 2014). Values for ONI were obtained from http://ggweather.com/enso/oni.htm for the months March–May. Similarly, the Pacific Decadal Oscillation (PDO) is a basin-scale pattern of ocean–atmosphere climate variability that can effect salmon production (Mantua, Hare, Zhang, Wallace, & Francis, 1997). This index is defined as the leading principal component of North Pacific monthly sea surface temperature anomalies' variability (poleward of 20°N for the 1900–1993 period). We downloaded PDO values from http://research.jisao.washington.edu/pdo/PDO.latest.txt for the months March–May. The North Pacific Gyre Oscillation (NPGO) is another mode of low-frequency climate variability associated with basin-scale ocean–atmosphere feedbacks (Di Lorenzo et al., 2010). The NPGO, defined as the second dominant mode of sea surface height anomalies in the central and eastern North Pacific, is associated with fluctuations in upper ocean salinity, nutrients, and a variety of other ecosystem indicators (Di Lorenzo et al., 2010). We downloaded PDO values from http://www.o3d.org/npgo/npgo.php for the months March–May. Sea level anomalies measured at tide gauges provide an indicator of alongshore geostrophic flow (Chelton, Bernal, & McGowan, 1982; Ralston, Sakuma, & Field, 2013). Positive sea level anomalies are proportional to poleward flows and negative anomalies with equatorward flows. We downloaded sea levels from a San Francisco tide gauge from https://tidesandcurrents.noaa.gov/sltrends/sltrends.html and calculated the mean annual sea level anomaly for March–May. Finally, we estimated the mean northward and eastward currents between 37.5° and 38.0°N (near the entrance to San Francisco Bay) from the ROMS model output discussed in section 2.2.

2.6 | Chinook salmon survival estimates

We used cohort reconstruction to estimate early survival of Chinook salmon using recoveries of hatchery fish implanted with coded-wire tags and released between 1988 and 2010 (Wells et al., 2017). Cohort reconstruction is a backward projection method that estimates numbers of fish that were available for capture based on the number captured and natural mortality (Magnusson & Hilborn, 2003). Hatchery salmon implanted with coded-wire tags were released throughout the Sacramento–San Joaquin watershed and recaptured as adults in the commercial fishery, recreational fishery, and as escapement (i.e., those fish that return to spawning habitats). To reduce variability due to size at release, only fingerlings' and advanced fingerlings' [mean weight = 6.32 g ± 0.19 *SE*] releases were used. We also restricted the analysis to fish released April through June during the period 1988–2010. We selected these years to coincide with the years available from the physical–biogeochemical model. For each coded-wire-tagged release group (n = 178), the total number of salmon released and the total number and dates of adult fish (>age 1) recovered from the Regional Mark Information System database (rmpc.org) were extracted. The range of the number of tagged fish released was 11,965 to 389,432 (mean = 46,708). The cohort reconstruction methods of Magnusson and Hilborn (2003) were followed to determine survival rates by estimating the number of individuals from a release group that survived to age 3 (N_3, two winters at sea):

$$N_3 = C_2S_2 + C_3 + (C_4/S_3) + (C_5/(S_3S_4)) + (C_6/(S_3S_4S_5)) \quad (2)$$

where C_a is the number of fish recovered at age a and S_a is survival rate at age a. As with Magnusson and Hilborn, survival rates following the first year at sea were assumed to be constant (S_2 = 0.6, S_3 = 0.7, S_4 = 0.8, S_5 = 0.9) and relatively minor components of the smolt-to-adult survival rate. The overall survival rate to age 3 for each release group was then estimated by dividing N_3 by the number of individuals released.

2.7 | Generalized linear model

A generalized linear model (GLM: Chambers & Hastie, 1993) was used to examine how the spatial variability in growth potential, represented by standardized NMS axis scores and overall growth potential, was related to the cohort reconstruction estimated survival rates (Section 2.1). The models were fit using a beta error distribution in the R package "betareg" because survival estimates are a proportional response (Cribari-Neto & Zeileis, 2010). The fully parameterized model included all potential interactions between the annual NMS axes scores and mean April - September growth potential throughout the study area. Interactive effects for all covariates (i.e., NMS axes scores and overall growth potential) were included in the fully parameterized model because the predictive effect of each covariate was expected to vary relative to the values of other covariates. In other words, we hypothesized that juvenile salmon survival depends on the interaction of multiple oceanographic processes that dictate the spatial distribution of growth potential. The full model was used to select the most appropriate link function, and the log-log link with no bias reduction was the most well supported based on Akaike's information criterion (AICc). We strongly suspected that we could not adequately estimate the 17 parameters in the full model with only 23 annual observations. Thus, we used AICc model selection to identify the most parsimonious model. All potential subsets of the full model were fit, and the model with the lowest AICc value was considered the most parsimonious model with the best fit to the observed survival estimates. Model selection was conducted using the R package "MuMIn" (Barton, 2018).

We used k-fold cross-validation to examine how well the model may perform when challenged with an out-of-sample data set. K-fold cross-validation involves dividing the full data set into k groups and iteratively using one of these groups to validate the predictions from a model fit to the remaining calibration data (Hastie, Tibshirani, & Friedman, 2009). To ensure we had a sufficient sample size to accurately assess the model predictions, we randomly selected validation data sets without replacement until the estimated survival for each year was based on a separate calibration data set. We repeated each

k-fold cross-validation process 100 times and examined the distribution of the beta regression pseudo r^2 values for the validation GLM survival estimates relative to the cohort reconstruction estimated survival.

3 | RESULTS

The physical–biogeochemical and bioenergetics models were used to estimate growth potential throughout the region where juvenile salmon were captured during a semi-annual trawl survey (Figure 2). The highest estimated growth potential values within our study area from 1988 to 2010 were within the Gulf of the Farallones (GoF; Figure 2a). There were also areas of higher growth in Monterey Bay and near Point Reyes. The area that was least favorable for growth was in the coastal waters north of Point Reyes. Trawl survey catches suggest that juvenile salmon are captured throughout the study area (Figure 2b), but are generally found distributed throughout the GoF and in nearshore waters north of Point Reyes (Hassrick et al., 2016); however, we note that trawls were not evenly distributed throughout the survey area and may not be a full representation of juvenile salmon distribution.

Three NMS axes sufficiently described the variability among the spatial cells across years. Stress for the final solution after 90 iterations was 0.048, indicating an excellent fit based on the rule of thumb provided by Clarke (1993). The proportion of variance represented by three axes between the original distance matrix and the ordination distances was R^2 = 0.99. Each NMS axis represented a different spatial pattern in growth variability, and all three axes were completely orthogonal. To maintain consistency, we rotated each of the three axes such that larger axis values represented higher growth potential within the spatial cells (Figure 3). The first NMS axis primarily represents growth variability within the GoF (Figure 3a). Growth potential in years with large Axis 1 values had higher growth potential within the GoF and near the shelf break. In contrast, years with low Axis 1 values had consistently low growth throughout the study area. The Axis 1 scores were positively correlated with the Bakun's upwelling index (0.64), NPGO (0.42), and NOI (0.46) and negatively correlated (−0.67) with the spring ONI (Table 1, Figure 4). The second NMS axis primarily represented variability in growth in the region just north of Point Reyes (Figure 3b). This axis was positively correlated (0.50) with the annual sea level anomaly at San Francisco, which provides an indicator of alongshore geostrophic flow (Table 1, Figure 4a). Finally, years with large Axis 3 values had higher growth potential in the most southern region of the study area (Figure 3c). Axis 3 was positively correlated (0.48) with the mean eastward velocity component and negatively correlated (−0.43) with the mean northward velocity component (Table 1, Figure 4b).

These axis scores, together with the mean April - September growth throughout the study area, explained much of the observed variability in juvenile salmon survival. Model selection overwhelmingly indicated that the most well-supported beta regression model included all the main effects as well as four-two-way interactions:

$$\begin{aligned} S_i = &\beta_0 + \beta_1 \text{Axis1}_i + \beta_2 \text{Axis2}_i + \beta_3 \text{Axis2}_i + \beta_4 \text{Growth}_i \\ &+ \beta_5 \text{Axis1}_i * \text{Axis2}_i + \beta_6 \text{Axis1}_i * \text{Axis3}_i + \beta_7 \text{Growth}_i * \text{Axis2}_i \\ &+ \beta_8 \text{Growth}_i * \text{Axis3}_i + \varepsilon_i \end{aligned} \quad (3)$$

where S_i is the cohort reconstruction estimated survival in year i, Axis 1, Axis 2, and Axis 3 are the NMS annual axis scores, Growth is the mean April - September growth, β_0–β_8 are model parameter estimates, and ε is the beta distributed residual error. This model was well supported as the top model (AICc weight = 0.75), with the next best model having a delta AICc of 6.10 (Table 2). The selected model had a pseudo r^2 of 0.82, indicating these predictor variables were able to explain much of the observed variability in juvenile Chinook survival throughout the time series (Figure 5). Cross-validation indicated that this model explained over half (r^2=0.51) the variation in early ocean survival during the ~4 years that were not used to fit the model. The individual cross-validation runs demonstrate that uncertainty increased during years with higher cohort reconstruction estimated survival (Figure 5a).

To understand how the parameters in the top GLM model affected model fit, we compared AICc values for GLM models that included, and excluded, a single covariate from the top model (Table 2). If the single parameter model included an interaction, we also included the main effects for that interaction. Likewise, we did not include any interaction that contained a main effect excluded from the model. For ease of interpretation, we will refer to the NMS axes by the oceanographic index with which they were most

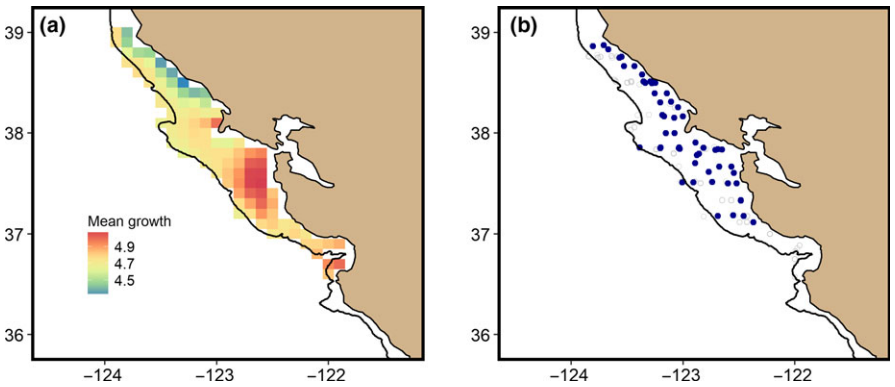

FIGURE 2 (a) Simulated juvenile Chinook salmon mean growth (g/day assuming a 150 g fish) based on a 23-year (1988–2010) run of the physical–biological fish model. (b) Survey trawl locations where juvenile salmon were either present (filled circles) or absent (empty circles) from 1997 to 2013

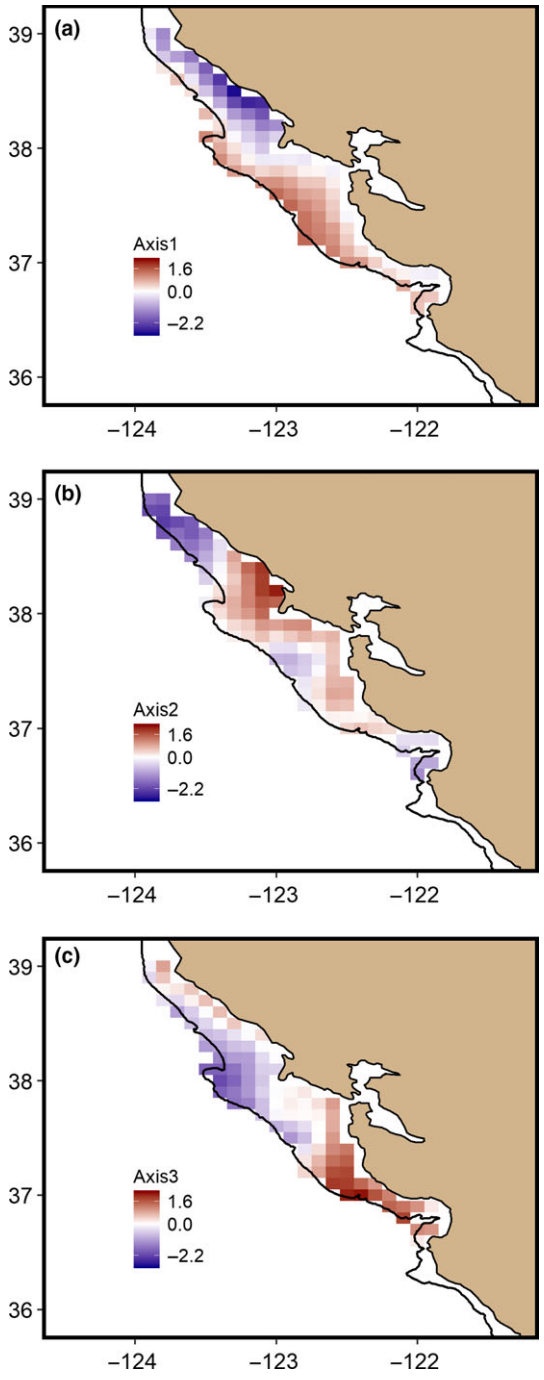

FIGURE 3 Standardized non-metric multidimensional scaling (NMS) axis scores within each spatial cell for (a) Axis 1, (b) Axis 2, and (c) Axis 3. Red and purple cells represent locations where growth potential was positively, and negatively, correlated with growth potential, respectively

positively correlated (i.e., Axis 1 = upwelling, Axis 2 = alongshore currents, and Axis 3 = across-shore currents), although this is an oversimplification. No single covariate or interaction produced a reasonable fit to the data. The best single covariate model included the interaction between upwelling and alongshore currents, but this model had a pseudo r^2 of only 0.32. Likewise, removal of the upwelling axis, and the interactions including the upwelling axis, resulted in the largest increase in AICc values. The top two missing covariate models were the ones that included both of the interactions with the across-shore currents axis. These models still had a reasonable fit to the data (pseudo r^2 = 0.69 and 0.63). This is understandable because these two interactions also had the largest standardized covariate values in the top model, and, thus, the most influence on the GLM estimated survival (Table 2).

To illustrate how different oceanic conditions (inferred from the NMS axes scores) influenced first-year survival rates, we plotted GLM predictions for each of the two-way interactions (Figure 6). For interpretation of how the nondimensional axis scores relate to the spatial distribution of growth potential and oceanographic conditions, refer to Figures 3 and 4. Positive values of Axis 1, indicative of increased upwelling conditions, generally corresponded with higher survival rates (Figure 4a,b). The lowest survival rates occurred when there was a combination of low values of Axis 1, representing anomalously weak upwelling associated with El Nino-like conditions (Jacox, Fiechter, Moore, & Edwards, 2015), and above average values for Axis 2, indicating increased poleward flow (Figure 4a), or Axis 3, indicating increased onshore flow (Figure 4b). Surprisingly, high growth potential throughout the study area did not consistently result in increased survival (Figure 4c,d). Once again, above average values of Axis 2 (Figure 4c) or Axis 3 (Figure 4d) resulted in decreased survival even when the mean growth potential throughout the study area was also above average. Based on the spatial distribution of growth potential (Figure 3), this implies that if mean growth potential is primarily concentrated just north of Point Reyes (Axis 2) or south of the GoF (Axis 3), there is reduced survival of juvenile salmon.

4 | DISCUSSION

We have demonstrated that annual spatial patterns in growth potential can be used to explain a considerable portion of the variation in juvenile Central Valley fall-run Chinook salmon survival. Spatially explicit growth potential was defined by the availability of mesoscale prey (i.e., krill) and water temperatures within the study area, which were both generated from a physical–biogeochemical model. Throughout the 23-year time series (1988–2010) examined in this study, juvenile salmon growth potential on the central California continental shelf was described by three spatial growth patterns identified by the NMS axes. These NMS axes, which represent different oceanographic conditions, were then included as covariates in a linear model to estimate survival. The most parsimonious linear model included interactions between the NMS axes and mean growth potential, indicating there is a complex relationship between spatial distribution in growth potential and salmon survival. It was particularly noteworthy that above average production throughout the study area did not necessarily result in higher survival, but was dependent on growth potential in specific regions. This finding suggests that regionally poor environmental conditions can be mitigated by local enhancement in growth potential (and vice versa) in the way

TABLE 1 Pearson correlations coefficients (r), and associated p-values, between oceanographic indices and NMS axes scores

	Axes 1		Axes 2		Axes 3	
Oceanographic index	***r***	***p***	***r***	***p***	***r***	***p***
Upwelling	**0.639**	**0.001**	−0.086	0.695	−0.013	0.954
ONI	**−0.673**	**<0.001**	0.176	0.421	−0.098	0.657
PDO	−0.220	0.312	0.219	0.315	0.139	0.529
NPGO	**0.423**	**0.044**	−0.314	0.144	−0.057	0.796
NOI	**0.462**	**0.027**	−0.288	0.183	0.111	0.613
Sea Level	−0.354	0.098	**0.503**	**0.015**	−0.112	0.612
Northward	−0.228	0.296	0.006	0.978	**−0.426**	**0.043**
Eastward	0.173	0.430	0.127	0.565	**0.482**	**0.020**

Note. Significant correlation coefficients ($p < 0.05$) are in bold.

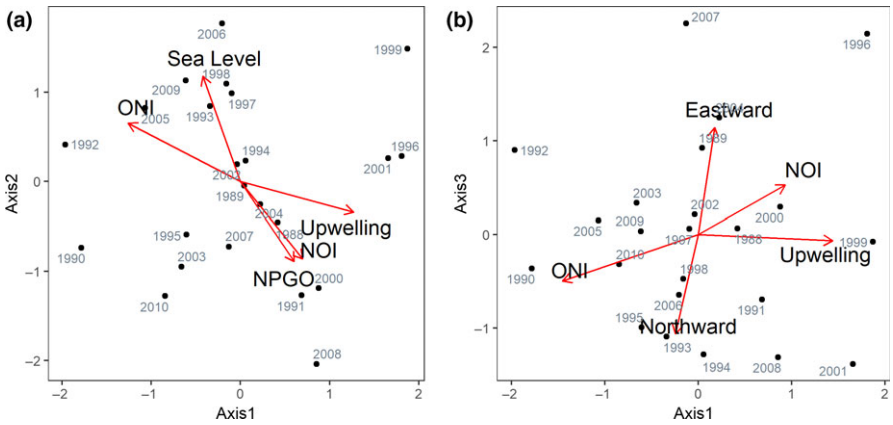

FIGURE 4 NMS plots showing the relative axis scores of each year in the time series (filled circles with gray labels) and the relationships between the axis scores and oceanographic conditions (red arrows and black labels). The direction of the arrow indicates whether the significant correlation ($p < 0.1$) is positive or negative, and the length of the arrow is proportional to the Pearson correlation coefficient

TABLE 2 Generalized linear model selection table with estimated β values for each covariate included in the top model, single covariate models, and missing covariate models

	Int	Axis 1	Axis 2	Axis 3	Growth	Axis 1: Axis 2	Axis 1: Axis 3	Axis 2: Growth	Axis 3: Growth	*k*	AICc	Delta AICc	Pseudo r^2
Top model	−1.55	0.10	−0.13	−0.11	−0.03	0.08	0.21	−0.09	−0.26	10	−178.54	0.00	0.82
Single covariate models	−1.59	0.03	−0.03			0.09				5	−172.45	6.09	0.32
	−1.57	0.04								3	−170.22	8.32	0.05
	−1.57			−0.01						3	−169.25	9.29	0.01
	−1.57				0.01					3	−169.24	9.30	0.01
	−1.57		−0.01							3	−169.09	9.46	0.00
	−1.58	0.03		−0.03			0.04			5	−165.79	12.75	0.11
	−1.56		−0.02		0.02			−0.04		5	−165.24	13.30	0.10
	−1.57			−0.02	0.02				−0.01	5	−163.33	15.21	0.03
Missing covariate models	−1.53	0.14	−0.11	−0.10	−0.08		0.24	−0.07	−0.29	9	−171.26	7.28	0.69
	−1.57	0.10	−0.12	−0.07	−0.02	0.08	0.16		−0.22	9	−167.98	10.57	0.63
	−1.58	0.02	−0.04		0.01	0.10		−0.05		7	−167.13	11.41	0.43
	−1.59	0.03	−0.03	−0.04		0.09	0.03			7	−167.06	11.48	0.36
	−1.59	0.01	−0.07	−0.10	0.05	0.12	0.05	−0.08		9	−166.74	11.81	0.56
	−1.58	0.00	−0.07	−0.07	0.05	0.12		−0.07	−0.03	9	−164.01	14.54	0.56
	−1.56	0.11		−0.03	−0.08		0.12		−0.14	7	−163.66	14.88	0.33
	−1.56		−0.04	−0.05	0.03			−0.06	−0.03	7	−160.03	18.51	0.16

Note. The "single covariate models" include one covariate (which includes the main effects if the single covariate is an interaction) from the top model. The "missing covariate model" excluded one covariate (which includes any interactions with that covariate) from the top model. Int is the intercept, Axis 1–Axis 3 are NMDS axis scores, Growth is the overall growth throughout the study area during the spring and summer, k is the number of parameters in the model, AICc is Akaike's information criterion, Delta AICc is the difference in AICc values from the top model, and the pseudo r^2 is the goodness of fit estimate from the generalized linear model.

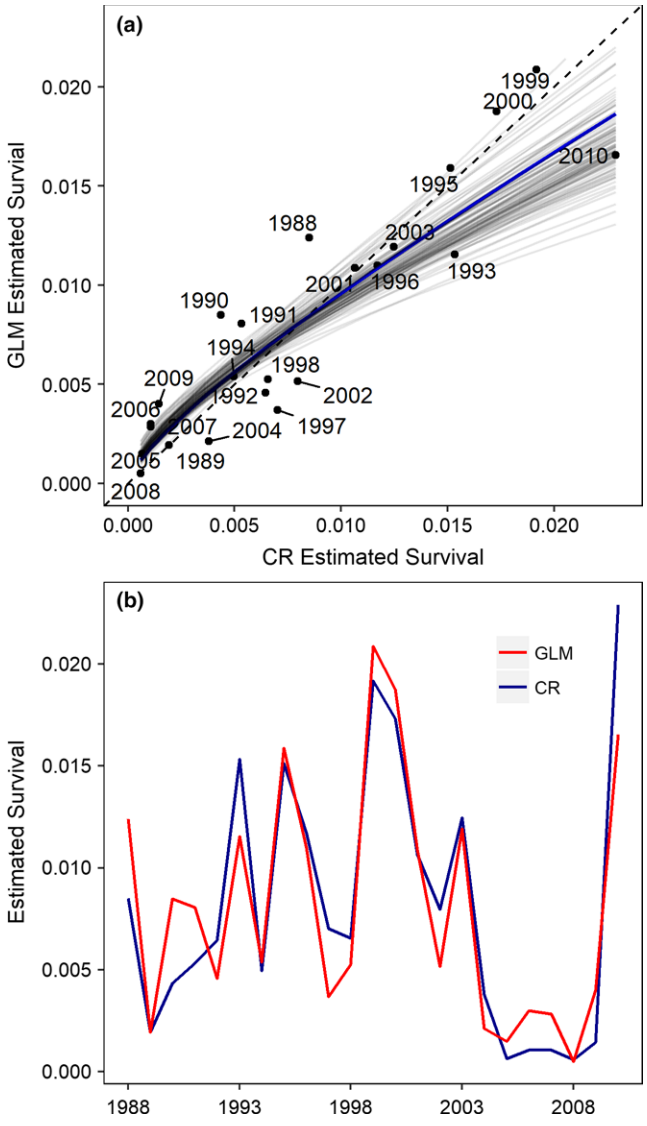

FIGURE 5 Juvenile Chinook salmon survival rates estimated from the cohort reconstruction (CR) and the generalized linear model (GLM). Data are displayed as both (a) a beta regression (blue line) and individual cross-validation model fits (gray lines), and (b) a time series (GLM—red line, CR—blue line)

it ultimately influences survival. The complex interplay between upwelling dynamics, coastal circulation patterns, and biological production as a determinant to juvenile salmon growth potential is also consistent with previously identified processes that produce mesoscale variability in krill distribution (Santora, Sydeman, Schroeder, Wells, & Field, 2011), forage fish availability (Santora, Schroeder, Field, Wells, & Sydeman, 2014), and predator foraging behavior (Wells et al., 2017).

The importance of upwelling, as captured by the first axis, is not surprising considering that the timing and strength of coastal upwelling in this region of the California Current Ecosystem is tightly related to overall production (Garcia-Reyes & Largier, 2012; Schroeder et al., 2014; Wells et al., 2016) and growth of salmon (Fiechter et al., 2015; Wells et al., 2012). A strongly positive amplitude of NMS Axis 1 was representative of years with higher growth potential within the GoF, which suggests both improved growth and expanded suitable habitat conditions in the region where juvenile salmon first out-migrate to sea when size-selective mortality is greatest (Woodson et al., 2013). Interestingly, NMS Axis 1 was also negatively correlated (−0.67) with the ONI during the months of juvenile salmon ocean entry. This implies that the modulation of coastal upwelling intensity by El Niño conditions, which are not independent of each other, influences salmon survival after ocean entry.

The second and third NMS axes were both correlated with oceanographic indices associated with oceanic currents. NMS Axis 2 was correlated with sea level anomalies measured at a San Francisco tide gauge. These sea level anomalies are associated with alongshore geostrophic flow (Chelton et al., 1982), and, thus, poleward–equatorward reversals of alongshore velocities were most likely the cause for the observed spatial distribution in growth potential. Years with high values of NMS Axis 2 had increased growth potential in the areas just north of Point Reyes, an area where juvenile salmon are often captured during the summer and fall after ocean entry (Hassrick et al., 2016). Thus, it makes sense that the highest observed survival rates were in years when both Axis 1 (upwelling) and Axis 2 (alongshore flow) were above average. Likewise, years with high values of NMS Axis 3 were associated with a stronger onshore component of the surface currents and had increased growth potential in the most southern regions of our study area. The standardized covariate estimates show that interactions with NMS Axis 3 had the largest impact on juvenile salmon survival. This is counterintuitive since juvenile salmon have been primarily captured north of the GoF during surveys (Hassrick et al., 2016). One hypothesis is that increased production to the south results in greater recruitment of forage fish (e.g., juvenile rockfish [*Sebastes* spp.], Pacific sardine [*Sardinops sagax*], and northern anchovy [*Engraulis mordax*]), hence decreasing predation pressure on juvenile salmon (Lindegren, Checkley, Rouyer, MacCall, & Stenseth, 2013; Wells et al., 2017).

Interestingly, all three of the spatial patterns that emerged from the analysis indicate that production within the GoF was important for salmon survival. This result implies that local retention mechanisms leading to improved growth conditions in the GoF can potentially mitigate regionally poor conditions during periods of weaker upwelling. This finding is also consistent with the results of Wells et al. (2012); in which it was demonstrated that consumption of krill within the GoF was the key aspect of improved growth, condition, and survival. Suitable growth conditions where juvenile salmon first enter the ocean will reduce the risk of size-selective mortality that can be significant when ocean conditions are poor (Tucker, Hipfner, & Trudel, 2016; Woodson et al., 2013), especially in the GoF when alternate prey species are less abundant (LaCroix et al., 2009; Wells et al., 2017).

A key result from our study is that no single spatial pattern of salmon growth potential could estimate salmon survival alone. This finding stresses the important notion that juvenile salmon survival

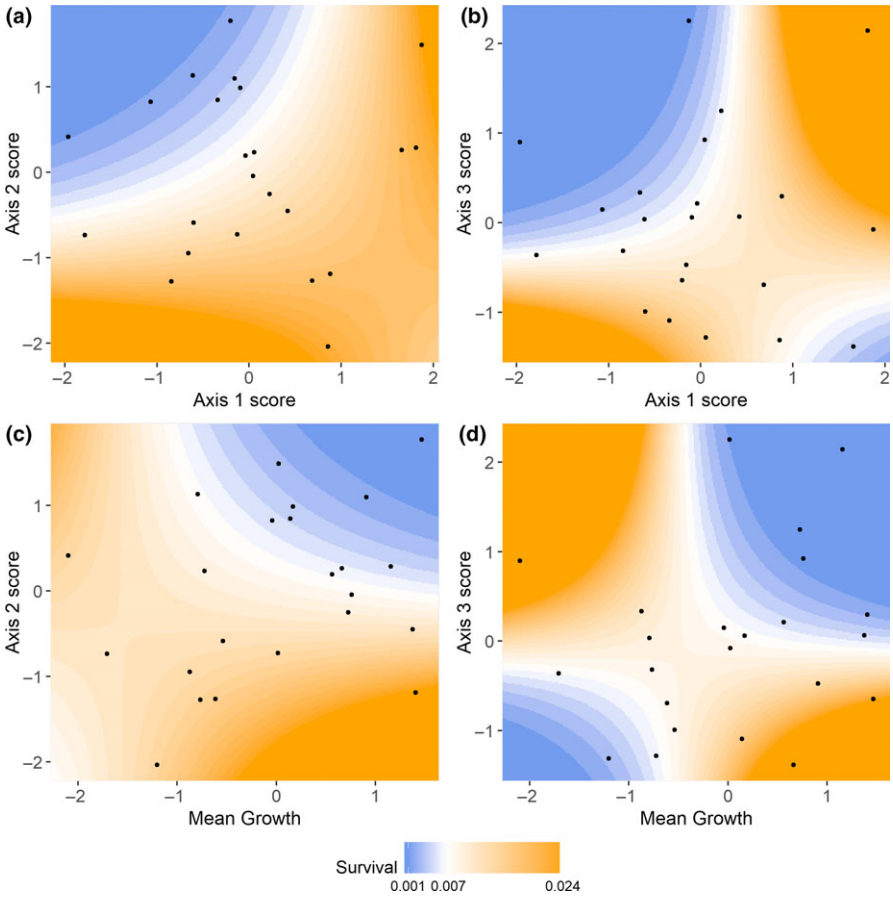

FIGURE 6 GLM model estimates of juvenile salmon survival for the four interactions included in the most parsimonious model, a) Axis 1 * Axis 2, b) Axis 1 * Axis 3, c) Mean April - Sept Growth * Axis 2, and d) Mean April - Sept Growth * Axis 3. These plots illustrate how survival varies relative to various combinations of oceanographic conditions. Orange and blue colors represent high and low ocean survival rates, respectively, based on model predictions. Overlaid on the contours is the NMS ordination for each year in our time series (filled circles)

is dependent on complex interactions between coastal upwelling dynamics, ocean circulation patterns, productivity, and prey availability. By including the interactions between spatial variations in growth potential in a linear model, we were able to explain over 80% of the variation in the estimates of survival based on tag returns. This model was most precise during years when estimated survival rates based on tag recaptures were lowest. This suggests that growth potential was generally a good predictor of survival when ocean conditions are poor, but other processes not included in our model could either increase or decrease survival when conditions were above a minimum threshold. This is not surprising as there is some uncertainty in our modeling effort. Because our estimates of survival were based on tag returns and have no associated confidence intervals, we were forced to assume these values are accurate; however, we know that changes in monitoring methods and reporting rates can affect tag return rates and the subsequent estimates of survival (Wells et al., 2017). Furthermore, our best generalized linear model estimated 10 parameters with only 23 annual survival estimates. Additional years of data should improve our model fit and our ability to infer how the interaction of oceanographic conditions influences juvenile salmon survival. Nonetheless, the approach we have demonstrated provides a means to estimate early ocean survival of juvenile salmon, which can dictate cohort strength, well before the adults return to spawn, providing invaluable information for fisheries managers.

Future work should focus on incorporating additional trophic levels into physical–biogeochemical–fish models (e.g., that of Fiechter et al., 2015). Recent research has found that juvenile salmon survival is dependent on both the forage available to juvenile salmon and predator density (Wells et al., 2017). However, the effect of predators on juvenile salmon survival was mitigated by the abundance of juvenile rockfish, the predators' preferred prey. We believe that a more fully integrated ecosystem approach, that incorporates predator abundance and the abundance of alternative forage fish (e.g., juvenile rockfish), will improve our ability to predict juvenile salmon survival rates.

ACKNOWLEDGEMENTS

This work was funded by grants from the National Science Foundation (OCE-1566623) and National Aeronautics and Space Administration (80NSSC17K0574). This paper is NOAA IEA program contribution #2018_7. Any opinions, findings, and conclusions or recommendations expressed here are those of the authors and do not necessarily reflect the views of the National Science Foundation. Brian Burke, Andre Buchheister, and Kathryn Sobocinski provided useful comments that greatly improved the manuscript. We thank the anonymous reviewers for their thoughtful comments. Any use of trade, firm, or product names is for descriptive purposes only and does not imply endorsement by the U.S. Government.

ORCID

Mark Henderson http://orcid.org/0000-0002-2861-8668

REFERENCES

Atlas, R., Hoffman, R. N., Ardizzone, J., Leidner, S. M., Jusem, J. C., Smith, D. K., & Gombos, D. (2011). A cross-calibrated, multiplatform ocean surface wind velocity product for meteorological and oceanographic applications. *Bulletin of the American Meteorological Society*, *92*, 157–174.

Bakun, A. (1973). *Coastal upwelling indices, West Coast of North America, 1946–71*. NOAA Tech Rep, NMFS SSRF-671, 114 pp.

Barton, K. (2018). MuMIn: Multi-Model Inference. R package version 1.40.4. https://CRAN.R-project.org/package=MuMIn

Beamish, R. J., & Mahnken, C. (2001). A critical size and period hypothesis to explain natural regulaiton of salmon abudnace and the linkage to climate and climate change. *Progress in Oceanography*, *49*, 423–435.

Crawford, W. J., Moore, A. M., Jacox, M. G., Fiechter, J., Neveu, E., & Edwards, C. A. (2017). A resonant response of the California Current circulation to forcing by low frequency climate variability. *Deep Sea Research Part II: Topical Studies in Oceanography*, *151*, 16–36.

Chambers, J. M., & Hastie, T. (1993). *Statistical models in S*. New York, NY: Chapman & Hall.

Chelton, D. B., Bernal, P. A., & McGowan, J. A. (1982). Large-scale interannual physical and biological interaction in the California Current. *Journal of Marine Research*, *40*, 1095–1123.

Clarke, K. R. (1993). Non-parametric multivariate analyses of changes in community structure. *Australian Journal of Ecology*, *18*, 117–143. https://doi.org/10.1111/j.1442-9993.1993.tb00438.x

Cribari-Neto, F., & Zeileis, A. (2010). Beta regression in R. *Journal of Statistical Software*, *34*, 1–24.

Di Lorenzo, E., Cobb, K. M., Furtado, J. C., Schneider, N., Anderson, B. T., Bracco, A., … Vimont, D. J. (2010). Central Pacific El Nino and decadal climate change in the North Pacific Ocean. *Nature Geoscience*, *3*, 762–765. https://doi.org/10.1038/ngeo984

Fiechter, J., Edwards, C. A., & Moore, A. M. (2018). Wind, circulation, and topographic effects on alongshore phytoplankton variability in the California Current. *Geophysical Research Letters*, *45*, 3238–3245.

Fiechter, J., Huff, D. D., Martin, B. T., Jackson, D., Edwards, C. A., Rose, K. A., … Wells, B. K. (2015). Environmental conditions impacting juvenile Chinook salmon growth off central California: An ecosystem model analysis. *Geophysical Research Letters*, *42*, 2910–2917. https://doi.org/10.1002/2015GL063046

Garcia-Reyes, M., & Largier, J. L. (2012). Seasonality of coastal upwelling off central and northern California: New insights, including temporal and spatial variability. *Journal of Geophysical Research-Oceans*, *117*, https://doi.org/10.1029/2011jc007629

Haidvogel, D. B., Arango, H., Budgell, W. P., Cornuelle, B. D., Curchitser, E., Di Lorenzo, E., … Wilkin, J. (2008). Ocean forecasting in terrain-following coordinates: Formulation and skill assessment of the Regional Ocean Modeling System. *Journal Computational Physics*, *227*, 3595–3624. https://doi.org/10.1016/j.jcp.2007.06.016

Harding, J. A., Ammann, A. J., & MacFarlane, R. B. (2011). Regional and seasonal patterns of epipelagic fish assemblages from the central California Current. *Fishery Bulletin*, *109*, 261–281.

Hassrick, J. L., Henderson, M. J., Huff, D. D., Sydeman, W. J., Sabal, M. C., Harding, J. A., … Hayes, S. A. (2016). Early ocean distribution of juvenile Chinook salmon in an upwelling ecosystem. *Fisheries Oceanography*, *25*, 133–146. https://doi.org/10.1111/fog.12141

Hastie, T. J., Tibshirani, R. J., & Friedman, J. H. (2009). The elements of statistical learning: data mining, inference, and prediction. 2nd ed., *Springer Series in Statistics* (2nd ed.). New York, NY: Springer.

Jacox, M. G., Fiechter, J., Moore, A. M., & Edwards, C. A. (2015). ENSO and the California Current coastal upwelling response. *Journal of Geophysical Research: Oceans*, *120*, 1691–1702.

Jacox, M. G., Moore, A. M., Edwards, C. A., & Fiechter, J. (2014). Spatially resolved upwelling in the California Current System and its connections to climate variability. *Geophysical Research Letters*, *41*, 3189–3196. https://doi.org/10.1002/2014GL059589

Jager, T., Martin, B. T., & Zimmer, E. I. (2013). DEBkiss or the quest for the simplest generic model of animal life history. *Journal of Theoretical Biology*, *328*, 9–18. https://doi.org/10.1016/j.jtbi.2013.03.01

Kilduff, D. P., Botsford, L. W., & Teo, S. L. H. (2014). Spatial and temporal covariability in early ocean survival of Chinook salmon (*Oncorhynchus tshawytscha*) along the west coast of North America. *ICES Journal of Marine Science*, *71*, 1671–1682. https://doi.org/10.1093/icesjms/fsu1031

Kishi, M. J., Kaeriyama, M., Ueno, H., & Kamezawa, Y. (2010). The effect of climate change on the growth of Japanese chum salmon (*Oncorhynchus keta*) using a bioenergetics model couples with a three-dimensional lower trophic ecosystem model (NEMURO). *Deep-Sea Research II*, *57*, 1257–1265. https://doi.org/10.1016/j.dsr2.2009.12.013

Kishi, M. J., Kashiwai, M., Ware, D. M., Megrey, B. A., Eslinger, D. L., Werner, F. E., … Zvalinsky, V. I. (2007). NEMURO – A lower trophic level model for the North Pacific marine ecosystem. *Ecological Modelling*, *202*, 12–25. https://doi.org/10.1016/j.ecolmodel.2006.08.021

Kruskal, J. B. (1964). Multidimensional scaling by optimizing goodness of fit to a nonmetric hypothesis. *Psychometrika*, *29*, 1–27. https://doi.org/10.1007/BF02289565

LaCroix, J. J., Wertheimer, A. C., Orsi, J. A., Sturdevant, M. V., Fergusson, E. A., & Bond, N. A. (2009). A top-down survival mechanism during early marine residency explains coho salmon year-class strength in southeast Alaska. *Deep-Sea Research Part I-Topical Studies in Oceanography*, *56*, 2560–2569. https://doi.org/10.1016/j.dsr2.2009.03.006

Lindegren, M., Checkley, D. M. Jr, Rouyer, T., MacCall, A. D., & Stenseth, N. C. (2013). Climate, fishing, and fluctuations of sardine and anchovy in the California Current. *Proceedings of the National Academy of Sciences of the United States of America*, *110*, 13672–13677. https://doi.org/10.1073/pnas.1305733110

Lindley, S. T., Grimes, C. B., Mohr, M. S., Peterson, W., Stein, J., Anderson, J. T., … Williams, T. H. (2009). What caused the Sacramento River fall Chinook stock collapse? NOAA Tech. Memo. NOAA-TM-NMFS-SWFSC-447.

MacFarlane, R. B. (2010). Energy dynamics and growth of Chinook salmon (*Oncorhynchus tshawytscha*) from the Central Valley of California during the estuarine phase and first ocean year. *Canadian Journal of Fisheries and Aquatic Sciences*, *67*, 1549–1565. https://doi.org/10.1139/F10-080

Mantua, N. J., Hare, S. R., Zhang, Y., Wallace, J. M., & Francis, R. C. (1997). A Pacific interdecadal climate oscillation with impacts on salmon production. *Bulletin of the American Meteorological Society*, *78*, 1069–1079. https://doi.org/10.1175/1520-0477(1997)078<1069:APICOW>2.0.CO;2

Mather, P. M. (1976). *Computational methods of multivariate analysis in physical geography*. London, UK: John Wiley and Sons.

Magnusson, A., & Hilborn, R. (2003). Estuarine influence on survival rates of coho (Oncorhynchus kisutch) and chinook salmon (Oncorhynchus tshawytscha) released from hatcheries on the U.S. Pacific coast. *Estuaries*, *26*, 1094–1103.

Michel, C. J., Ammann, A. J., Lindley, S. T., Sandstrom, P. T., Chapman, E. D., Thomas, M. J., … MacFarlane, R. B. (2015). Chinook salmon

outmigration survival in wet and dry years in California's Sacramento River. *Canadian Journal of Fisheries and Aquatic Sciences*, *72*, 1749–1759. https://doi.org/10.1139/cjfas-2014-0528

Moore, A. M., Arango, H. G., Broquet, G., Powell, B. S., Zavala-Garay, J., & Weaver, A. T. (2011). The Regional Ocean Modeling System (ROMS) 4-dimensional variational data assimilation systems, Part I: Formulation and Overview. *Progress in Oceanography*, *91*, 34–49. https://doi.org/10.1016/j.pocean.2011.05.004

Neveu, E., Moore, A. M., Edwards, C. A., Fiechter, J., Drake, P., Crawford, W. J., … Nuss, E. (2016). An historical analysis of the California Current circulation using ROMS 4D-Var: System Configuration and diagnostics. *Ocean Modelling*, *99*, 133–151.

Null, J. (2017). *El Nino and La Nina years and intensities: based on Oceanic Nino Index (ONI)*. Retrieved from http://ggweather.com/enso/oni.htm. Accessed 15 December 2017.

Oksanen, J., Blanchet, F. G., Friendly, M., Kindt, R., Legendre, P., McGlinn, D., & Wagner, H. (2017). *vegan: Community Ecology Package*. R package version 2.4-2. R. CRAN.

Peterson, W. T., Fisher, J. L., Peterson, J. O., Morgan, C. A., Burke, B. J., & Fresh, K. L. (2014). Applied fisheries oceanography: Ecosystem indicators of ocean conditions inform fisheries management in the California Current. *Oceanography*, *27*, 80–89. https://doi.org/10.5670/oceanog

R Core Team (2016). *R: A language and environment for statistical computing*. Vienna, Austria: R Foundation for Statistical Computing.

Ralston, S., Sakuma, K. M., & Field, J. C. (2013). Interannual variation in pelagic juvenile rockfish (Sebastes spp.) abundance – going with the flow. *Fisheries Oceanography*, *22*, 288–308. https://doi.org/10.1111/fog.12022

Santora, J. A., Schroeder, I. D., Field, J. C., Wells, B. K., & Sydeman, W. J. (2014). Spatio-temporal dynamics of ocean conditions and forage taxa reveals regional structuring of seabird-prey relationships. *Ecological Applications*, https://doi.org/10.1890/1813-1605.1891

Santora, J. A., Sydeman, W. J., Schroeder, I. D., Wells, B. K., & Field, J. C. (2011). Mesoscale structure and oceanographic determinants of krill hotspots in the California Current: Implications for trophic transfer and conservation. *Progress in Oceanography*, *91*, 397–409. https://doi.org/10.1016/j.pocean.2011.04.002

Schroeder, I. D., Santora, J. A., Moore, A. M., Edwards, C. A., Fiechter, J., Hazen, E. L., Bograd, S. J., … Wells, B. K. (2014). Application of a data-assimilative regional ocean modeling system for assessing California Current System ocean conditions, krill, and juvenile rockfish interannual variability. *Geophysical Research Letters*, *41*, 5942–5950.

Schwing, F. B., O'Farrell, M., Steger, J. M., & Baltz, K. (1996). *Coastal upwelling indices, West Coast of North America, 1946–1995*. NOAA Tech Memo, NOAA-TM-NMFS-SWFSC-231, 144.

Shchepetkin, A. F., & McWilliams, J. C. (2005). The regional oceanic modeling system (ROMS): A split-explicit, free-surface, topography-following-coordinate oceanic model. *Ocean Modelling*, *9*, 347–404. https://doi.org/10.1016/j.ocemod.2004.08.002

Stewart, D. J., & Ibarra, M. (1991). Predation and production by salmonine fishes in Lake Michigan, 1978-88. *Canadian Journal of Fisheries and Aquatic Sciences*, *45*, 909–922.

Tucker, S., Hipfner, J. M., & Trudel, M. (2016). Size- and condition-dependent predation: A seabird disproportionately targets substandard individual juvenile salmon. *Ecology*, *97*, 461–471. https://doi.org/10.1890/15-0564.1

Wells, B. K., Santora, J. A., Field, J. C., MacFarlane, R. B., Marinovic, B. B., & Sydeman, W. J. (2012). Population dynamics of Chinook salmon *Oncorhynchus tshawytscha* relative to prey availability in the central California coastal region. *Marine Ecology Progress Series*, *457*, 125–137. https://doi.org/10.3354/meps09727

Wells, B. K., Santora, J. A., Henderson, M. J., Warzybok, P., Jahncke, J., Bradley, R. W., … Ainley, D. G. (2017). Environmental conditions and prey-switching by a seabird predator impacts juvenile salmon survival. *Journal of Marine Systems*, *174*, 54–63. https://doi.org/10.1016/j.jmarsys.2017.05.008

Wells, B. K., Santora, J. A., Schroeder, I. D., Mantua, N., Sydeman, W. J., Huff, D. D., & Field, J. C. (2016). Marine ecosystem perspectives on Chinook salmon recruitment: A synthesis of empirical and modeling studies from a California upwelling system. *Marine Ecology Progress Series*, *552*, 271–284. https://doi.org/10.3354/meps11757

Woodson, L. E., Wells, B. K., Weber, P. K., MacFarlane, R. B., Whitman, G. E., & Johnson, R. C. (2013). Size, growth, and origin-dependent mortality of juvenile Chinook salmon *Oncorhynchus tshawytscha* during early ocean residence. *Marine Ecology Progress Series*, *487*, 163–175. https://doi.org/10.3354/meps10353

Yoon, S., Watanabe, E., Ueno, H., & Kishi, M. J. (2015). Potential habitat for chum salmon (*Oncorhynchus keta*) in the Western Arctic based on a bioenergetics model coupled with a three-dimensional lower trophic ecosystem model. *Progress in Oceanography*, *131*, 146–158. https://doi.org/10.1016/j.pocean.2014.12.009

How to cite this article: Henderson M, Fiechter J, Huff DD, Wells BK. Spatial variability in ocean-mediated growth potential is linked to Chinook salmon survival. *Fish Oceanogr*. 2018;00:1–11. https://doi.org/10.1111/fog.12415